

Investigation of multilayer X-ray optics for the 6 keV to 20 keV energy range

P. Oberta,^{a,b*} Y. Platonov^c and U. Flechsig^d

Received 28 February 2012

Accepted 14 July 2012

^aRigaku Innovative Technologies Europe, Novodvorská 994, 142 21 Praha 4, Czech Republic, ^bInstitute of Physics of the Academy of Sciences of the Czech Republic, Na Slovance 2, 182 21 Praha 8, Czech Republic, ^cRigaku Innovative Technologies Inc., 1900 Taylor Road, Auburn Hills, MI 48326, USA, and ^dSwiss Light Source, Paul Scherrer Institut, CH-5232 Villigen, Switzerland. E-mail: oberta@fzu.cz

The X-ray optics group at the Swiss Light Source in co-operation with RIT (Rigaku Innovative Technologies) have investigated seven different multilayer samples. The goal was to find an ideal multilayer structure for the energy range between 6 keV and 20 keV in terms of energy resolution and reflectivity. Such multilayer structures deposited on substrates can be used as X-ray monochromators or reflecting synchrotron mirrors. The measured reflectivities agree with the simulated ones. They cover a reflectivity range from 45% to 80% for energies between 6 keV and 10 keV, and 80% to 90% for energies between 10 keV and 20 keV. The experimentally measured energy resolution of the samples lies between 0.3% and 3.5%.

© 2012 International Union of Crystallography
Printed in Singapore – all rights reserved

Keywords: X-ray optics; multilayer; energy resolution.

1. Introduction

Multilayer (ML) optics plays an important role in the X-ray optics family. It all began at the beginning of the 1970s (Spiller, 1972), when the first 'layered synthetic micro-structure' was used for Bragg-case diffraction optics for soft X-rays (Haelbach & Kunz, 1976; Barbee, 1981; Underwood & Barbee, 1981). One of the reasons for the wider use of ML optics being restricted at that time was the substrate quality and to a certain extent the quality of the ML itself. This all changed with the development of new polishing technologies reaching low surface roughness and slope errors. At the same time the first third-generation synchrotron facilities started to operate. The flux of the third-generation facilities was several orders of magnitude higher compared with the previous generation. Flux conservation began to play an important role in X-ray optics. For an X-ray monochromator, two properties are crucial: energy resolution and reflectivity or flux. In the first case, crystal monochromators have no serious competition and reach the highest resolution among monochromators. In the second case, MLs deliver higher flux owing to the broader bandwidth compared with crystal monochromators. Therefore many beamlines, preferring flux over resolution, started to use ML monochromators and ML optics in general. Comparing with mirrors, the grazing angle for ML optics is higher, thus the total length of the optics is shorter. Furthermore the *d*-spacing of a ML structure can be tailored for a specific application, making it more flexible compared with crystal optics. ML optics started to be investigated and developed at several synchrotron facilities, such as CHESS (Bilderback,

1982; Smolenski *et al.*, 1998; Kazimirov *et al.*, 2006) and ESRF (Deschamps *et al.*, 1995; Morawe *et al.*, 2001). New deposition technologies and choice of material promise higher performances (Honnicke *et al.*, 2010; Jahedy *et al.*, 2010). ML optics is also a promising candidate for sub-nanometer focusing (Kang *et al.*, 2007; Mimura *et al.*, 2010).

This manuscript describes an extensive experimental investigation of seven different ML structures (see Table 1). Based on these results a proper ML structure can be chosen for optimal performance in the given energy range. The investigation was performed in the frequently used energy range between 6 keV and 20 keV. The choice of ML material was determined by the optical properties in the considered photon energy range.

2. Deposition of the multilayers

Double-crystal monochromators (DCMs) are common optical devices at synchrotron facilities. Crystals are typically used as spectral selective elements. Artificial ML structures came to replace crystals when an application did not require high selectivity but there was a demand for higher flux. Another advantage of a ML is that different structures can be deposited on a single substrate to cover a wide spectral range with optimal performance. This is called a multi-stripped DMM (double-multilayer monochromator). For optimal performance the multilayers should satisfy requirements on *d*-spacing, peak reflectivity and resolution. There is typically a trade-off between throughput and resolution of a DMM.

Table 1

Parameters of the deposited ML structures.

d is the period, σ_{avg} is the average ‘effective’ interfacial roughness through the ML stack, γ is the thickness ratio of the first material layer to the total period, N is the number of periods, Θ is the Bragg angle, R is the peak reflectivity and $\text{FWHM}/\tan \Theta$ is the relative energy bandwidth.

Sample	d (nm)	Cu $K\alpha$ 1st-order reflectivity			Θ (°)	R (%)	FWHM/ $\tan \Theta$ (%)
		σ_{avg} (nm)	γ [$h(1\text{st})/d$]	N			
Ru/B ₄ C	2.83	0.26	0.41	170	1.59	71.5	1.22
Ni/B ₄ C	4.52	0.35	0.47	100	1.02	91.4	2.63
SiC/B ₄ C	5.30	0.40	0.30	300	0.86	43.9	1.32
W/B ₄ C	1.50	0.27	0.30	300	2.96	57.7	0.52
V/B ₄ C	3.02	0.29	0.26	300	1.48	56.9	0.77
V/B ₄ C	2.30	0.28	0.28	500	1.93	48.3	0.48
Ti/B ₄ C	4.01	0.25	0.30	250	1.13	60.3	1.08

Larger d -structures deliver higher flux but lower resolution in comparison with smaller d -structures. The choice of multilayer materials is an important step in DMM design. Optimal optical properties are the main criteria in choosing the best material combination for a multilayer design. Another criteria is how well selected materials can form smooth and sharp interfaces. In the frame of this work we deposited and investigated the X-ray performance of multilayer structures based on different pairs of materials with different d -values and different spectral resolution. The purpose was to determine the most promising multilayers for the photon energy range from 6 keV to 20 keV.

The multilayers were deposited at RIT (Rigaku Innovative Technologies) on flat 1-inch-diameter silicon substrates (Fig. 1), by using conventional magnetron sputtering technology (Platonov *et al.*, 1997). Six different pairs of materials, *i.e.* Ru/B₄C, Ni/B₄C, SiC/B₄C, V/B₄C, Ti/B₄C and W/B₄C, were coated. The V/B₄C structure was deposited with two d -spacings of 2.3 nm and 3.0 nm. All Ru/B₄C and Ni/B₄C multilayers were coated using an in-line deposition system allowing us to deposit structures of up to 1.5 m in length. The remaining multilayers were deposited using a carousel-type system where the substrates are mounted on facets of a rotating carousel which pass in front of the magnetron sputtering sources to form an alternating structure. The desired thickness of the coatings for each material was obtained through control of the rotational period of the carousel or the

translation speed of a carrier on the in-line system. Ion-beam sources were used on both machines for cleaning the substrates prior to deposition.

The substrates were delivered from Gooch & Housego (formerly General Optics). High-spatial-frequency roughness of the substrate surface was measured using a Veeco DI3100 atomic force microscope viewing a 10 μm \times 10 μm scanning area. Mid-spatial frequency roughness was tested using a Zygo New View 6300 interferometric microscope with different magnifica-

tions. The approach used for surface roughness characterization was described in detail by Martynov & Platonov (2008). A typical power spectral density (PSD) function of the 1-inch substrates is presented in Fig. 2. Surface roughness was calculated from the PSD to be about 0.1 nm r.m.s.

3. Performance calculations and X-ray measurement

3.1. Cu $K\alpha$ testing at RIT

All the samples were measured with a Cu $K\alpha$ tube at the RIT and at the optics beamline (X05DA) at the Swiss Light Source (SLS) (Flechsigs *et al.*, 2009). After deposition, the multilayers were characterized using a modified Huber Cu $K\alpha$ diffractometer. Θ – 2Θ scans were performed in the angular range from grazing incidence to the highest observable reflection-order angle. The probe beam divergence was 17 arcsec. A typical reflectivity curve is presented in Fig. 3. Based on the measured Bragg angle position, peak reflectivity and peak width the authors estimated the d -spacing, relative thickness of the layers, material densities of the layers and ‘effective’ roughness. The effective roughness includes such imperfections of the multilayers as interlayer diffusion and actual roughness between the layers. The calculated parameters of the deposited structures are presented in Table 1.



Figure 1
The Si substrate on which the ML structure was deposited.

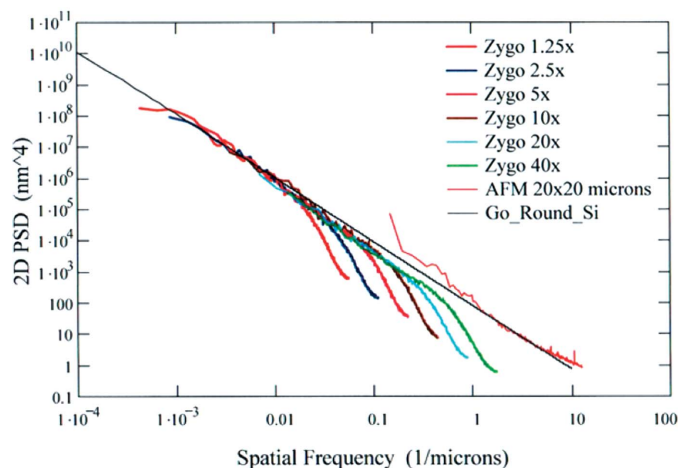


Figure 2
Summary PSD function of a typical substrate.

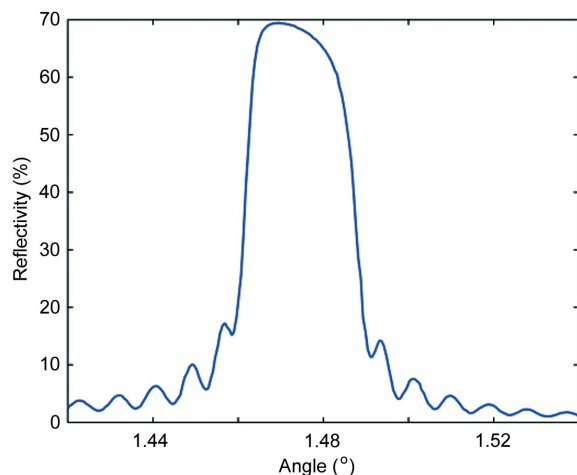


Figure 3
 Θ - 2Θ reflectivity curve at Cu $K\alpha$ from the V/B₄C ML structure with $d = 3.017$ nm. The divergence of the probe beam is 17 arcsec.

The multilayer d -spacing varied from 1.5 nm for W/B₄C structures to 5.3 nm for SiC/B₄C structures. The number of periods for each structure was selected to achieve maximum peak reflectivity from 6 keV to 20 keV. The multilayer parameters found from Cu $K\alpha$ performance were used to calculate the expected reflectivity in the working photon energy range. These calculations were carried out by using the *IMD* program developed by Windt (1998). Plane waves with no divergence were considered. The expected peak reflectivity and resolution of the deposited multilayers are presented in Figs. 4 and 5, respectively. For most of the multilayers the dependence of reflectivity on photon energy is expected to be smooth across the energy range of interest. Exceptions are for the W/B₄C and Ni/B₄C structures which show sharp changes in reflectivity at energies corresponding to the W-L and Ni-K absorption edges. The data in Fig. 4 show that a high level of reflectivity is

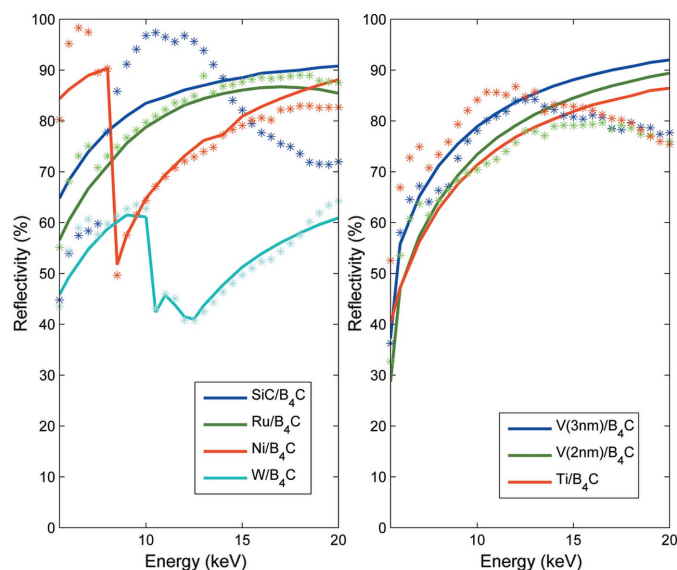


Figure 4
 Calculated peak reflectivity of the deposited MLs ranging from 6 keV to 20 keV. The *IMD* program was used. Calculations were performed for plane waves.

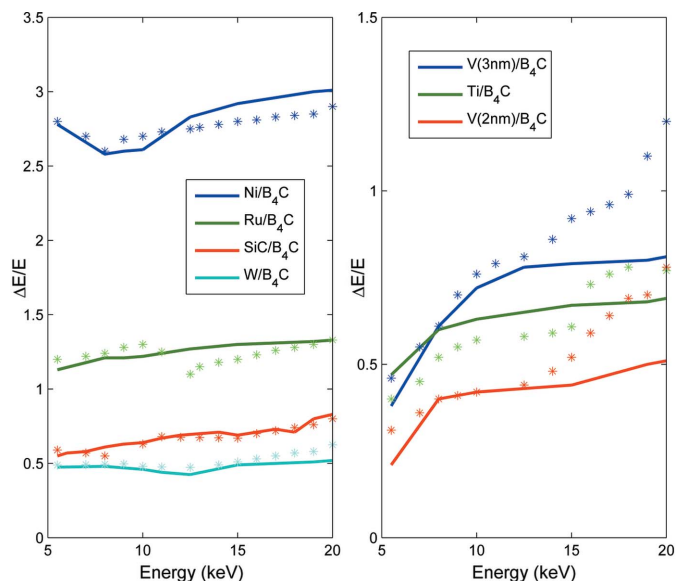


Figure 5
 Calculated resolutions of the deposited MLs ranging from 6 keV to 20 keV. The *IMD* program was used. Calculations were performed for plane waves.

achievable in any energy interval inside the 6 keV to 20 keV range. For instance, Ni/B₄C is the best candidate for the interval from 6 keV to 8 keV; W/B₄C is the most promising up to 10 keV; above 10 keV all remaining structures look promising. Resolution is relatively uniform across the full spectral range for any given multilayer; however, energy resolution varies from 0.3% to 3.5% depending on the d -spacing. The resolution numbers correlate very well with d -spacing: a larger d -value results in lower resolution. One exception exists among the considered structures: SiC/B₄C with $d = 5.3$ nm. The expected energy resolution for this multilayer is 0.6%, well below the 1.5% for Ru/B₄C with $d = 2.8$ nm and 3.5% for Ni/B₄C with $d = 4.5$ nm. The reason for this exception in energy resolution is that SiC/B₄C is a structure based on low contrast and low absorptive materials. As a result, the reflection process is built from the effective contribution of many layers owing to the deep penetration of X-ray radiation into the multilayer stack.

All deposited multilayers contain boron carbide material as one of the layers. B₄C-based structures are typically quite stable at the high temperatures expected from the high heat load in synchrotron applications. The thermal stability of the deposited structures was tested at temperatures up to 533 K. The multilayers were annealed for 1 h at 323 K, 373 K, 423 K, 473 K and 533 K in a vacuum oven. After each annealing cycle the multilayers were tested on a Cu $K\alpha$ diffractometer. Figs. 6 and 7 present the d -spacing and reflectivity change measured at Cu $K\alpha$ radiation as a function of the annealing temperature. All structures showed a slight reduction of d -spacing at 323 K. From 323 K upwards, d -spacing tends to increase with temperature. The Ni/B₄C structure appears most stable while V/B₄C multilayers demonstrated the largest increase of d -value. The largest d -spacing change observed after annealing at the highest temperature of 533 K was from 0.2% for Ni/B₄C

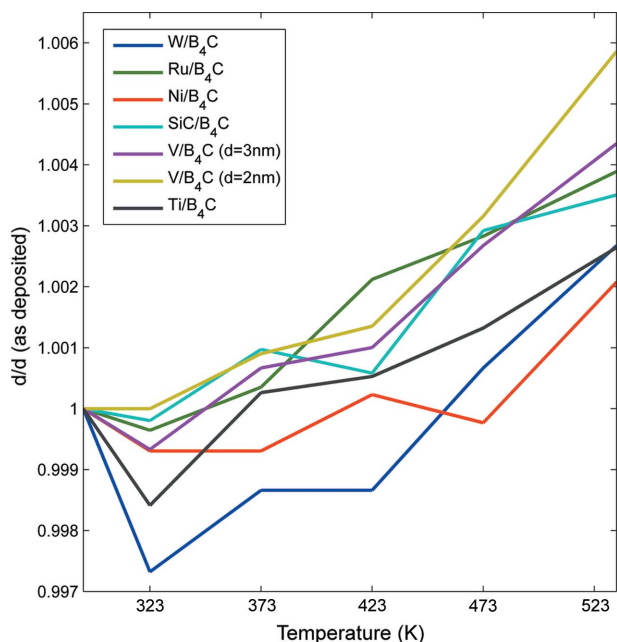


Figure 6 Change in d -spacing of B_4C -based MLs as a function of annealing temperature.

with $d = 4.5$ nm to 0.6% for V/B_4C with $d = 2.3$ nm. The measured change in d -spacing as a function of annealing temperature has a fixed error bar of ± 0.00085 . To make the plot in Fig. 6 more transparent we did not include the error bars. Reflectivity did not show a noticeable trend while increasing annealing temperature. The maximum variation in the reflectivity was $\pm 5\%$ which is in agreement with the reflectivity measurement accuracy of the particular $Cu K\alpha$ diffractometer used. The error bars in this measurement were ± 0.05 .

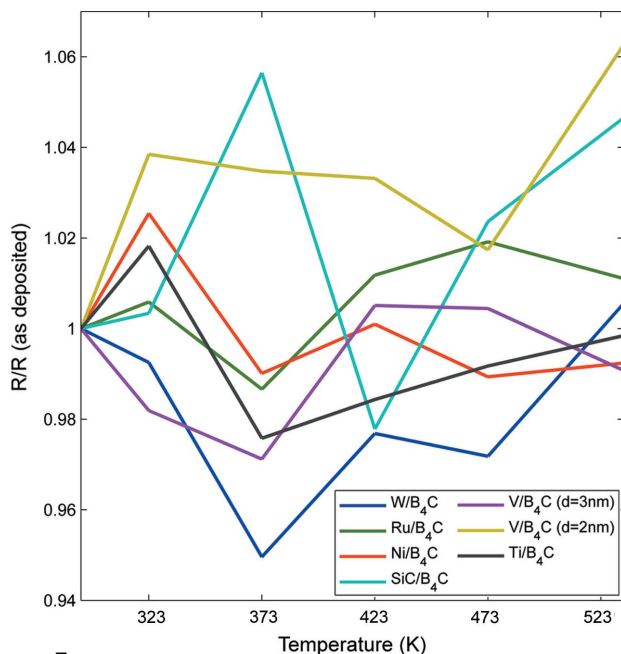


Figure 7 First-order $Cu K\alpha$ reflectivity of B_4C -based MLs as a function of annealing temperature.

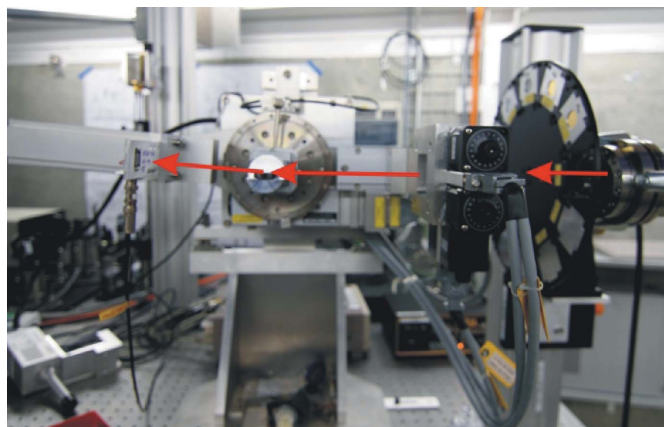


Figure 8 Experimental set-up: low-vacuum tube, slits, sample holder with sample, and a Si pin-diode.

3.2. Synchrotron measurements at the SLS

The reflectivity measurements were performed at the optics beamline (X05DA) at the SLS. The experimental set-up is shown in Fig. 8. We glued the sample using a chemical glue to the holder which was mounted on the Θ arm of the goniometer. As a detector a silicon photodiode (AXUV100) with a quadratic area of 1 cm^2 was used and mounted on the 2Θ arm of the goniometer. A slit system, standing downstream of the sample, was opened to $0.5\text{ mm} \times 0.5\text{ mm}$. A focused monochromatic beam with a focal spot size of $140\text{ }\mu\text{m} \times 70\text{ }\mu\text{m}$ ($H \times V$) was used. The SLS beamlines are operated *via* the EPICS (Experimental Physics and Industrial Control System) control system. A special tool developed for other reasons (Flechsigt *et al.*, 2010) was used to perform the Bragg angle (Θ_B) adjustment. By defining the d -spacing as the only free parameter, the tool is able to set for a given energy the goniometer sample holder to the Θ_B angle and the goniometer arm to the $2\Theta_B$ angle. To scan the whole energy range and to scan around the Bragg angle a two-dimensional scan was performed. The inner scan scanned the diffraction peak around Θ_B at a given energy. The outer scan scanned the whole energy range between 6 keV and 20 keV in 500 eV steps (two-dimensional scan). Two-dimensional maps were obtained (Fig. 9) for every sample. From these maps the diffraction peak for every energy step can be extracted.

To visualize the intensity distribution, the two-dimensional map was plotted in false colours (Fig. 9). The intensity distribution inherits all the conditions of the experimental set-up, like bending-magnet spectrum and beam absorption in air. The y -axis is the scanned angle around the Bragg peak, the x -axis is the scanned energy range and the colour bar represents the reflected intensity. The absorption edge of Ni at 8.33 keV is represented by the drop of intensity (green/yellow area between the red areas). The curvature of the plot is due to refraction. The effect of refraction is stronger for lower energies than for higher energies; therefore the Bragg peak for lower energies deviates more strongly. The difference in the deviation of the Bragg peak between 6 keV and 20 keV is only about 100 arcsec (0.031°). The acquired reflectivity plots are

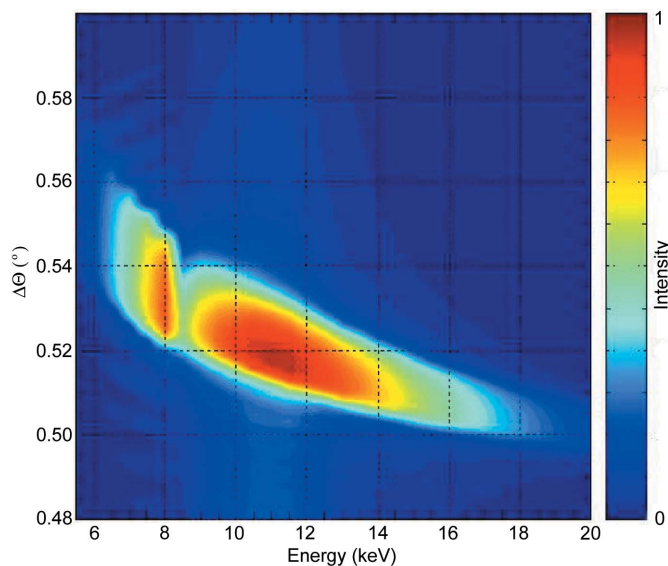


Figure 9
Two-dimensional map of Ni/B₄C ML. The intensity drop at 8.33 keV is the absorption edge of Ni. The plot curvature is due to refraction.

shown in Fig. 10. The two plots show the expected and the measured reflectivity. The full line is the expected reflectivity and the stars represent the measured reflectivity points. The expected reflectivity is described in §3.1. It is the reflectivity obtained from the ML parameters found from the Cu K α performance. The measured reflectivity curves of Ni/B₄C, Ru/B₄C and W/B₄C are almost identical to the expected ones. The small maximum in the reflectivity curve at the beginning of the plot is due to higher harmonics of the bending-magnet source (Flechsig *et al.*, 2009). There is a 17% contamination at 6 keV from the third harmonic. Absorption edges can also be observed in the reflectivity plots: at 8.33 keV the K₁-edge of nickel (Ni/B₄C), and at 10.2 keV, 11.5 keV and 12 keV the L₁-, L₂- and L₃-edges of tungsten (W/B₄C). The only sample with a

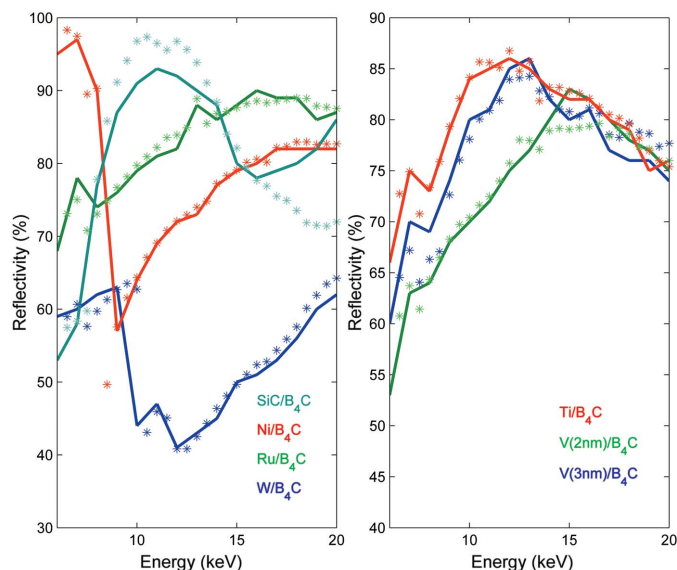


Figure 10
Reflectivity plots of the ML samples. Full lines represent the expected reflectivity and the stars represent the measured reflectivity points.

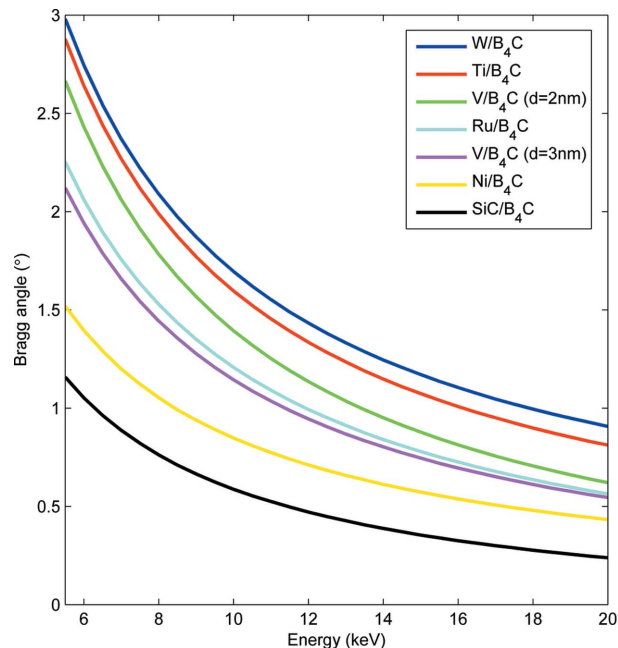


Figure 11
Bragg angle *versus* energy for seven investigated ML samples.

different measured reflectivity compared with the expected one is SiC/B₄C. In the lower and higher energy range the experimentally measured reflectivity is lower, but in the middle of the energy range the reflectivity is a little bit higher. The origin of the mismatch between the measured and expected reflectivity curve is unknown. Fig. 11 shows the dependence of Bragg angle on energy for all seven measured samples. The Bragg angles cover a wide range beginning as low as 0.25° to almost 3°. The Bragg angle depends on the *d*-spacing value.

Figs. 12 and 13 show the investigated energy resolution, $\Delta E/E$, of the ML samples. For MLs, as for crystals, the resolution is determined by the width of the diffraction curve, $\Delta\Theta$. The corresponding formula is

$$\Delta E/E = \Delta\Theta \cot \Theta_B, \quad (1)$$

where Θ_B is the Bragg angle. Based on the achieved energy resolution there are three major groups of ML optics. The first group are high-energy-resolution MLs with $\Delta E/E \simeq 0.1\%$; these MLs cover the gap between normal-energy-resolution MLs and crystal monochromators. The second group are the traditional MLs with an energy resolution of $\Delta E/E \simeq 2\%$, and the last group are wide-bandpass MLs with an energy resolution of $\Delta E/E > 5\%$ (Flechsig *et al.*, 2010). The MLs investigated by our group can be placed between the traditional and the high-resolution MLs. As seen from Figs. 12 and 13, the highest energy resolution, around 0.5%, is reached by W/B₄C, V/B₄C (*d* = 2.3 nm), Ti/B₄C and SiC/B₄C samples. The energy resolution of V/B₄C (*d* = 3 nm) is from 0.4% to 1.0%. The remaining two samples, Ni/B₄C and Ru/B₄C, can be placed between the traditional MLs. The energy resolution of Ru/B₄C is between 1.1% and 1.3% and the energy resolution of Ni/B₄C is between 2.6% and 3.0%. From the measured data

(using the measured Bragg angle at a given energy) one can also extract the d -spacing value and compare it with the estimated one. Table 2 compares the tabulated d -spacing values measured at SLS and the estimated ones. For the Ru/B₄C, W/B₄C and the V/B₄C ($d = 3$ nm) samples the variation is less than 5%; for the Ni/B₄C, SiC/B₄C and the V/B₄C ($d = 2$ nm) samples the variation is below 9%. Only the Ti/B₄C sample has a variation of 21% between the measured and the estimated d -spacing.

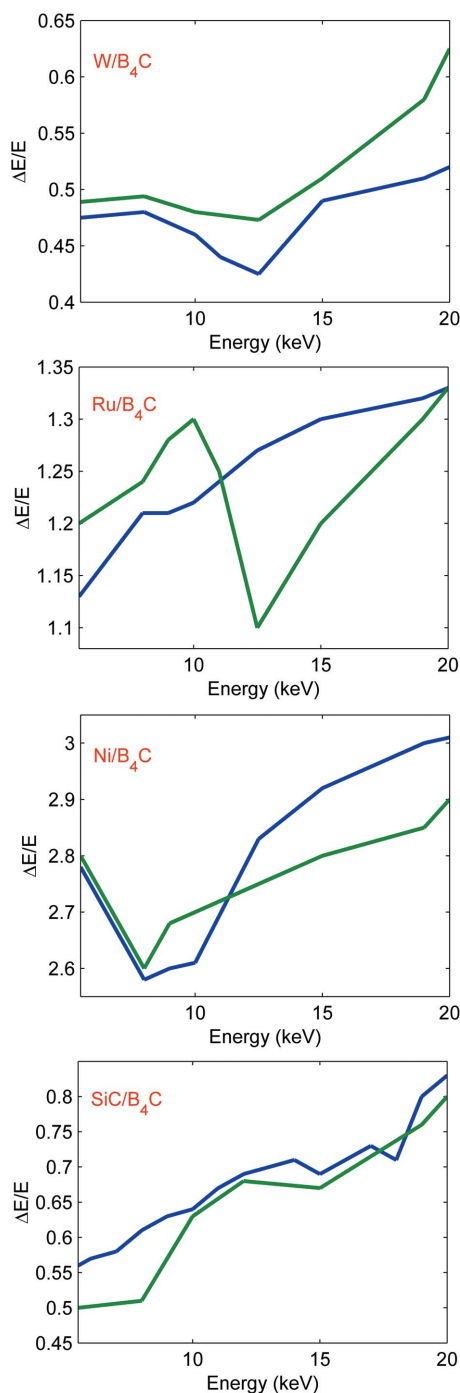


Figure 12 Resolution of the ML samples. The blue line represents the expected values and the green line the experimental values.

Table 2 d -spacing comparison (default units: nm).

N is the number of periods on the substrate and Δ (%) is the deviation of the d -spacing from the measured and estimated value.

Sample	d (Rigaku)	d (SLS)	Δ (%)	N
Ru/B ₄ C	2.83	2.90	2.41	170
Ni/B ₄ C	4.52	4.21	7.36	100
SiC/B ₄ C	5.30	5.82	8.93	300
W/B ₄ C	1.50	1.57	4.70	300
V/B ₄ C	3.02	3.08	1.98	300
V/B ₄ C	2.30	2.49	8.20	500
Ti/B ₄ C	4.01	3.31	21.0	250

spacing value and calculating the Bragg diffraction angles for the whole energy range gives a constant offset value of $\sim 0.14^\circ$.

4. Conclusion

Seven different ML samples were investigated in terms of reflectivity measurement and resolution calculations. The

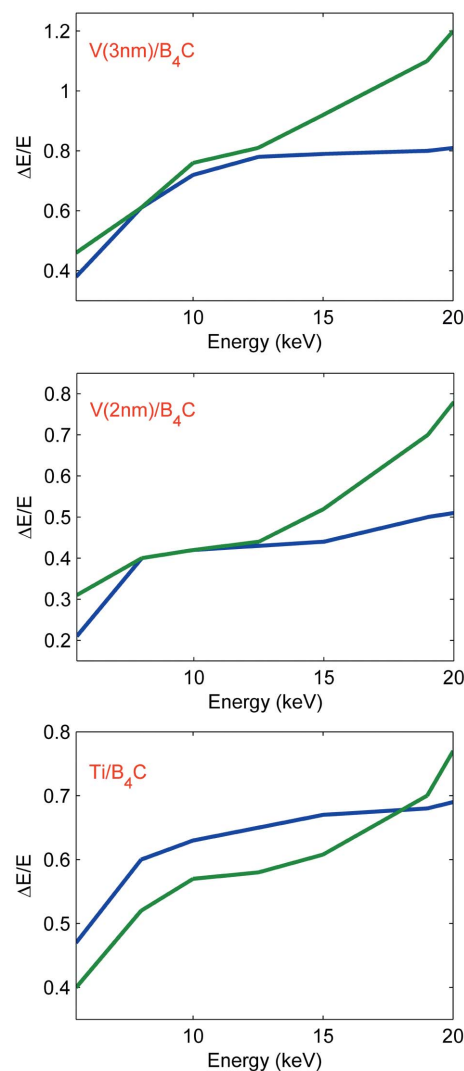


Figure 13 Resolution of the ML samples. The blue line represents the expected values and the green line the experimental values.

measured data are very similar to the expected one. Both reflectivity and d -spacing were investigated as a function of the annealing temperature. The obtained results will be used for an optimization process for ML X-ray optics. The achieved energy resolutions (0.5–3%) and the reflectivities (60–95%) show a high potential for the investigated ML structures in the field of X-ray optics. The mismatch in the reflectivity plots can be due to the experimental set-up. Raw intensity data were used for the plots, without investigating the influence of the bending-magnet spectrum or absorption. The latter could influence the high-energy reflectivity. The reason for the disagreement between the measured and expected resolution is unknown. This shows that, in addition to the optical properties of ML structures simulated by a computer code, there is still a need for X-ray metrology measurements as confirmation.

References

- Barbee, T. W. (1981). *AIP Conf. Proc.* **75**, 131–145.
- Bilderback, D. H. (1982). *Nucl. Instrum. Methods*, **195**, 67–72.
- Deschamps, P., Engström, P., Fiedler, S., Riekkel, C., Wakatsuki, S., Høghøj, P. & Ziegler, E. (1995). *J. Synchrotron Rad.* **2**, 124–131.
- Flechsigt, U., Jaggi, A., Spielmann, S., Padmore, H. A. & MacDowell, A. A. (2009). *Nucl. Instrum. Methods Phys. Res. A*, **609**, 281–285.
- Flechsigt, U., Nielsen, J. A., Jaggi, A., Krempasky, J., Oberta, P., Spielmann, S. & van der Veen, J. F. (2010). *AIP Conf. Proc.* **1234**, 653–656.
- Haelbach, R. P. & Kunz, C. (1976). *Opt. Commun.* **17**, 287–292.
- Honnicke, M. G., Huang, X., Keister, J. W., Kodituwakku, C. N. & Cai, Y. Q. (2010). *J. Synchrotron Rad.* **17**, 352–359.
- Jahedy, N., Conley, R., Shi, B., Qian, J., Lauer, K. & Macrander, A. (2010). *Nucl. Instrum. Methods Phys. Res. A*, **616**, 89–92.
- Kang, H. Ch., Stephenson, G. B., Liu, Ch., Conley, R., Khachatryan, R., Wieczorek, M., Maclander, A. T., Yan, H., Maser, J., Hiller, J. & Koritala, R. (2007). *Rev. Sci. Instrum.* **78**, 046103.
- Kazimirov, A., Smilgies, D.-M., Shen, Q., Xiao, X., Hao, Q., Fontes, E., Bilderback, D. H., Gruner, S. M., Platonov, Y. & Martynov, V. V. (2006). *J. Synchrotron Rad.* **13**, 204–210.
- Martynov, V. & Platonov, Y. (2008). *Proc. SPIE*, **7077**, 707704.
- Mimura, H., Handa, S., Morawe, Ch., Yokoyama, H., Kimura, T., Matsuyama, S. & Yamauchi, K. (2010). *Nucl. Instrum. Methods Phys. Res. A*, **616**, 251–254.
- Morawe, C., Peffen, J. C., Ziegler, E. & Freund, A. K. (2001). *Proc. SPIE*, **4145**, 61–71.
- Platonov, Y., Broadway, D., DeGroot, B., Verman, B., Keem, B., Gutman, G., Wood, J., Rodriguez, J. & Grupido, N. (1997). *Proc. SPIE*, **3152**, 231–239.
- Smolenski, K. W., Headrick, R. L., Shen, Q., Carroll, B., Khounsary, A. M., Liu, C. & Maclander, A. T. (1998). *Proc. SPIE*, **3448**, 27–31.
- Spiller, E. (1972). *Appl. Phys. Lett.* **20**, 365–367.
- Windt, D. L. (1998). *Comput. Phys.* **12**, 360–370.
- Underwood, J. H. & Barbee, T. W. (1981). *Appl. Opt.* **20**, 3027–3034.